



BUCK CONTROLLER IMPLEMENTATION USING A80803 WITH SLEW-RATE CONTROL FOR 48 V AUTOMOTIVE LED HEADLIGHT APPLICATIONS

By Vashist Bist and Shashank Wekhande, Systems Engineers
Allegro MicroSystems

ABSTRACT

The need for more-power-efficient systems in automotive applications has triggered a trend-shift from the 12 V battery to the 48 V battery. This shift enables hybridization with better fuel economy and reduced emissions at low cost. In applications such as headlights, taillights POS/daytime running lights (DRLs), this shift necessitates high-voltage LED controllers to minimize the power losses that result from adapting the 48 V source to 12 V applications.

This application note considers automotive high-power/high-voltage applications where a smaller number of LEDs are driven at a battery voltage of 48 V (with maximum operating voltage at 56 V, supporting 70 V load dump) using the Allegro multi-topology synchronous LED controller (A80803). A design procedure is also detailed, including device behavior during steady-state operation, transient analysis, slew-rate control in various modes, and behavior with various protection features.

INTRODUCTION

The A80803 is a constant-current DC-DC switching controller for high-power automotive lighting applications. The controller is based on a programmable fixed-frequency, peak-current-mode control architecture and can be configured in multiple different switching topologies to suit different application requirements. The device includes both low-side and high-side gate drivers to control the external power MOSFETs. Moreover, two additional gate drivers are integrated to enable/disable part of the LED string to simplify high-/low-beam applications.

Diagnostics can be reported through SPI or via the two fault pins. The SPI interface can also be used to control many configuration options of the A80803. Alternatively, these options can be factory-programmed and stored in EEPROM to remove the need for a local microcontroller.

LED brightness can be controlled by a pulse-width-modulated (PWM) signal on the EN/PWM pin or by an internal PWM sig-

nal configured via SPI. An internal driver controls a MOSFET in series with the LED string to optimize dimming. The PWMOUT driver strength is programmable via SPI to optimize LED current during PWM transitions. LED current foldback is provided for low-input voltage and thermal events.

The buck converter implementation with the A80803 device with slew-rate control is shown in Figure 1. The buck converter is implemented using a low-side switch (SW_1) and a free-wheeling synchronous switch (SW_2). Two PMOS switches are used for the PWM dimming (SW_p) and high-beam/low-beam operation (SW_{lb}). A slew-rate control is implemented using a differential amplifier (Op_1) which provides a scaled output of the LED voltage (i.e., voltage between anode and cathode).

High-beam or low-beam operation can be achieved by either turning on all LEDs (six LEDs) in a string or turning on only a few LEDs (four LEDs) and short-circuiting the rest. The low-beam operation is achieved by turning on the bypass-MOSFET (SW_{lb}) controlled with the LBG node. Due to the limited response time of the power-stage controller, LEDs may experience a large deviation in the current during high-/low-beam transitions. It is important to minimize these LED current deviations to eliminate any undesirable flicker. LED current deviations during high/low-beam transitions can be minimized by slowing the turn-on and turn-off rates of the bypass MOSFET (SW_{lb}). The slew-rate control is achieved using the SLEW pin, the input of which is supplied by a differential amplifier (LED string voltage is input to the differential amplifier) and two slew components (R_{SLEW} and C_{SLEW}) that determine the rate of transition, as discussed in the Design Procedure section.

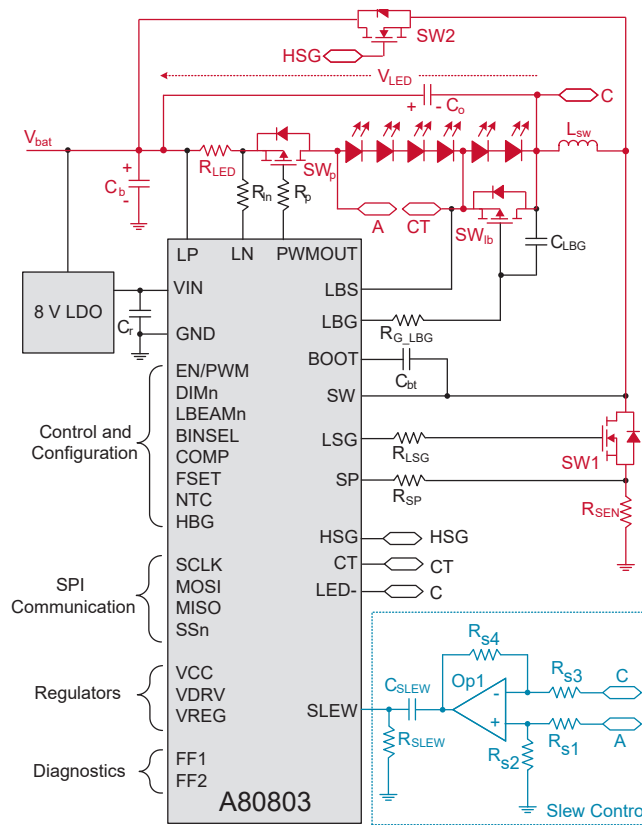


Figure 1: High-voltage buck configuration using A80803.

OPERATION

The simplified power stage of a buck converter in continuous-conduction mode (CCM) is shown in Figure 2. The waveform of the buck converter in CCM is shown over a complete switching cycle in Figure 3. Buck-converter operation during switch-on and switch-off is as follows:

Mode 1 (switch turn-on): During the switch (SW) turn-on period (t_{ON}), energy is stored in the inductor (L_{SW}) while supplying the LED current, as shown in Figure 2 (b). The inductor current ($I_{L_{SW}}$) increases, and the output voltage (V_{LED}) changes depending on the direction of the output-capacitor current, as shown in Figure 3.

Mode 2 (switch turn-off): During the switch turn-off period (t_{OFF}), the diode (D_{SW}) conducts, and the inductor (L_{SW}) provides the required energy to the LEDs to maintain a continuous current, as shown in Figure 2 (c). The inductor current ($I_{L_{SW}}$) reduces, as shown in Figure 3. The output capacitor (C_{out}) helps in the reduction of ripple current.

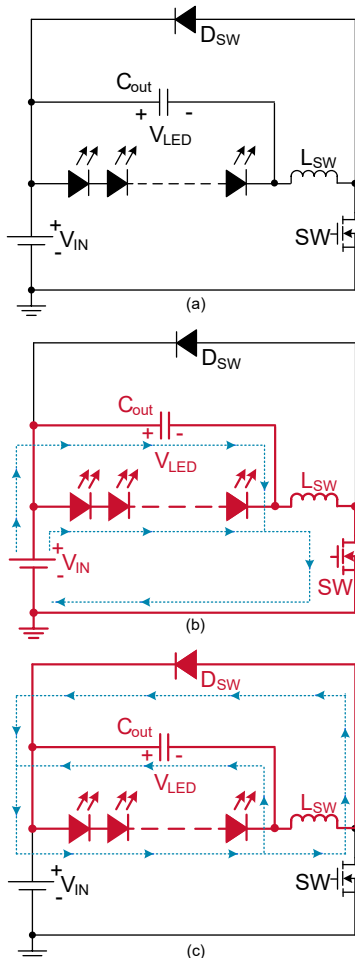


Figure 2: Buck converter: (a) simplified power stage, (b) operation during the switch-on period, and (c) operation during the switch-off period.

Considering the input voltage (V_{IN}), LED voltage (V_{LED} , output voltage), and switch turn-on and turn-off times (t_{ON} and t_{OFF} , respectively), the volts-per-second balance across inductors (L_{SW}) in continuous-conduction mode as:

Equation 1:

$$(V_{IN} - V_{LED}) \times t_{ON} = V_{LED} \times t_{OFF}$$

which can be rearranged as:

Equation 2:

$$V_{IN} \times t_{ON} = V_{LED} \times (t_{ON} + t_{OFF})$$

On- and off-time can be replaced as a function of duty (D) as:

Equation 3:

$$V_{LED} = \frac{t_{ON}}{(t_{ON} + t_{OFF})} \times V_{IN} = D \times V_{IN}$$

This is a typical buck-converter equation showing how output voltage (V_{LED}) is linked with the input voltage (V_{IN}).

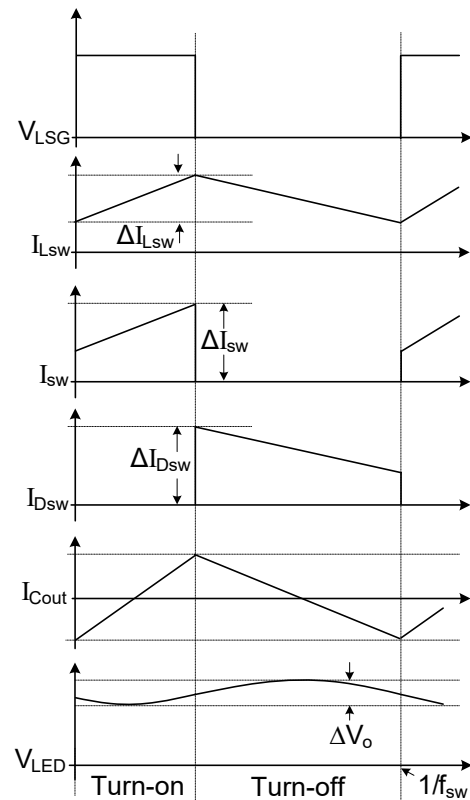


Figure 3: Waveforms of the operation of the buck converter in continuous-conduction mode (CCM).

DESIGN PROCEDURE

Power Components

Considering the on-time period as shown in in Figure 2 (b), the voltage across inductor, V_{Lon} , is given as:

Equation 4:

$$V_{Lon} = L \frac{d}{dt_{ON}}(I_{LSW}) = (V_{IN} - V_{LED})$$

Substitution of Equation 3 in Equation 4 results in:

Equation 5:

$$V_{Lon} = L_{SW} \frac{d}{dt_{ON}}(I_{LSW}) = (V_{IN} - D \times V_{IN})$$

$$\Rightarrow L_{SW} \frac{\Delta I_{LSW}}{Dt} = V_{IN} (1 - D)$$

Using Equation 5, the value of the inductor is expressed as:

Equation 6:

$$L_{SW} = \frac{V_{IN} D (1 - D)}{\Delta I_{LSW} f_{SW}} = \frac{V_{LED} (1 - D)}{\Delta I_{LSW} f_{SW}}$$

Moreover, the output capacitor is designed as:

Equation 7:

$$C_{OUT} = \frac{\Delta I_{LSW}}{8 \times f_{SW} \times \Delta V_{Cout}}$$

where, ΔI_{LSW} is the peak-to-peak ripple current in the inductor, ΔV_{Cout} is the peak-to-peak voltage ripple across the output capacitor, and f_{sw} is the PWM switching frequency. Both the inductor (L_{SW}) and the output capacitor (C_{OUT}) must be designed at the maximum input voltage.

Slew-Rate Control

This section presents the design procedure of the slew-rate control circuitry for the A80803.

Due to buck configuration, the shorting of MOSFET is to be carried out by the LBG MOSFET because this configuration requires a floating gate driver or a PMOS. For further details about the slew-rate control, refer to the A80803 datasheet.

The operating input voltage of the A80803 driver is limited to 37 V; it cannot be powered directly from the 48 V battery. Moreover, the primary condition for the LBG MOSFET to slew requires the input voltage (V_{IN}) to be lower than the voltage at the CT terminal (V_{CT}).^[1]

The voltage at the CT terminal (V_{CT}) is calculated as the difference between the minimum supply voltage and the voltage across the high-beam LED string:

Equation 8:

$$V_{CT} = V_{IN} - V_{LED_{HB}}$$

where $V_{LED_{HB}}$ is the voltage across the LED string from anode to CT node.

Hence, to power the input-voltage (V_{IN}) pin of the A80803—which maintains the input voltage (V_{IN}) of the A80803 such that it is always lower than the voltage at VCT for the slew-rate control of the LBG MOSFET, and such that it meets the maximum supply-voltage requirement for the A80803 device—a low-dropout regulator (LDO) is connected.

The slew-rate circuitry of the buck converter, which comprises a differential amplifier and a differentiator, is shown in Figure 4. Because the voltage at the CT terminal (VCT) is almost constant during transitions between low- and-high beam operation, a differential amplifier is able to provide an inverted, scaled differential output of the LED string voltage (from anode to cathode). Therefore, a differential amplifier is used to provide feedback of the LED voltage that needs to be slewed. Finally, as a feedback signal to the A80803 device, the RC differentiator provides the rate-transitioned output of the SLEW pin.

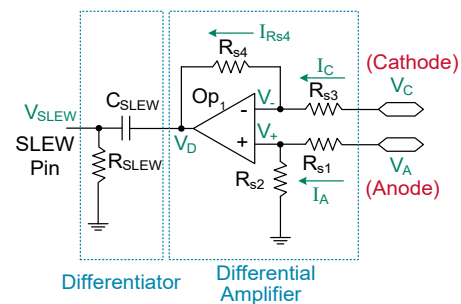


Figure 4: Slew-rate control circuitry

The design of various components of the differential amplifier is as follows.

The voltage at the noninverting input (V+) is expressed as:

Equation 9:

$$V_+ = V_A \left(\frac{R_{S2}}{R_{S1} + R_{S2}} \right)$$

The amplifier output (V_{D(V-)}) in the inverting-amplifier configuration, when V_A = 0,

Equation 10:

$$V_{D(V-)} = - \left(\frac{R_{S4}}{R_{S3}} \right) V_C$$

Considering the amplifier output (V_{D(V+)}) in the noninverting amplifier configuration, when V_C = 0:

Equation 11:

$$V_{D(V+)} = \left(1 + \frac{R_{S4}}{R_{S3}} \right) V_+$$

The value of (V+) obtained in Equation 11 can then be substituted into Equation 4 to obtain:

Equation 12:

$$V_{D(V+)} = \left(1 + \frac{R_{S4}}{R_{S3}} \right) \left(\frac{R_{S2}}{R_{S1} + R_{S2}} \right) V_A$$

The superposition theorem can then be used to express the differential amplifier output as:

Equation 13:

$$V_D = V_{D(V+)} + V_{D(V-)}$$

Hence, Equation 10 and Equation 11 can be substituted into Equation 13 to produce:

Equation 14:

$$V_D = \left(1 + \frac{R_{S4}}{R_{S3}} \right) \left(\frac{R_{S2}}{R_{S1} + R_{S2}} \right) V_A - \left(\frac{R_{S4}}{R_{S3}} \right) V_C$$

Considering six LEDs (~19.8 V typical LED voltage) in the high-beam operation and four LEDs (~13.2 V typical LED voltage) in the low-beam operation, with anode voltage as 48 V, the cathode voltage is calculated as 28.2 V and 34.8 V for high-beam and low-beam operation, respectively.

Considering, the case such that R_{S1} = R_{S3} and R_{S2} = R_{S4}, Equation 14 can be rearranged as:

Equation 15:

$$V_D = \left(\frac{R_{S4}}{R_{S3}} \right) (V_A - V_C) = A_d \times (V_A - V_C),$$

where A_d is the gain of the differential amplifier.

The values of R_{S1} = R_{S3} = 100 kΩ, and R_{S2} = R_{S4} = 15 kΩ can then be substituted into Equation 15 to produce:

Equation 16:

$$V_D = A_d \times (V_A - V_C) = 0.15 \times (V_A - V_C).$$

Using Equation 16, the gain of the differential amplifier (A_d) is calculated as 0.15.

Also using Equation 16, the differential voltage in high-beam (V_{D_HB}) and low-beam (V_{D_LB}) operation is calculated as:

Equation 17:

$$V_{D_HB} = 0.15 \times (48 - 28.2) = 2.97V; \text{ and}$$

Equation 18:

$$V_{D_LB} = 0.15 \times (48 - 34.8) = 1.98V.$$

As shown in Equation 17 and Equation 18, the output voltage of the differential amplifier is higher than the SLEW pin threshold of 250 mV and there is sufficient margin for LED voltage variation. Also, the output voltage swing (i.e., V_{D_HB} - V_{D_LB}) is approximately 1 V, which is sufficient for effective slew-rate detection. For different system configurations, select the differential amplifier gain (A_D) such that V_{D(V+)} is less than the supply voltage to the differential comparator and maximizes the differential output voltage swing.

Moreover, the SLEW pin is designed such that the rate of slew control is defined by the RC differentiator as:

Equation 19:

$$\frac{dV}{dt} (V/ms) = \frac{250(mV)}{R_{SLEW}(k\Omega) \times C_{SLEW}(nF)},$$

where R_{SLEW} and C_{SLEW} are components shown in Figure 4 and 250 mV is the internal voltage threshold of the SLEW pin.

Because LED voltage is fed through a differential amplifier, the differential amplifier gain is used to calculate the actual slew as:

Equation 20:

$$\frac{dV_{LED}}{dt} (V/ms) = \frac{250(mV)}{A_d \times R_{SLEW}(k\Omega) \times C_{SLEW}(nF)}.$$

Using Equation 20, the slew rate is calculated for R_{SLEW} of 5 kΩ and C_{SLEW} of 47 nF and 100 nF as:

Equation 21:

$$\frac{dV_{LED}}{dt} (@47nF) = \frac{250}{0.15 \times 5 \times 47} = 7.09V/ms; \text{ and}$$

Equation 22:

$$\frac{dV_{LED}}{dt} (@100nF) = \frac{250}{0.15 \times 5 \times 100} = 3.33V/ms.$$

Hence, by adjusting the component values of the differentiator, the slew rate can be adjusted.

Design and selection of other components and configuration of various features is available in the datasheet. [1]

STEADY-STATE OPERATION

This section presents the steady-state operation of the buck controller implemented using the A80803 device.

The efficiency and LED current plots with respect to the input voltage are shown in Figure 5 and Figure 6, respectively. The system depicts high efficiency and good LED current regulation at varying input voltage.

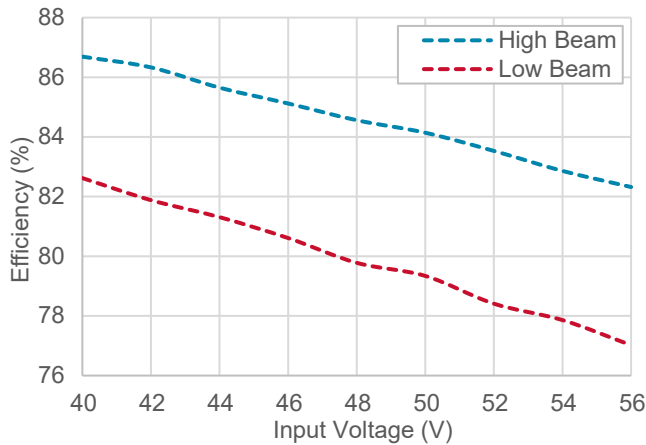


Figure 5: Efficiency vs. input voltage for high-beam and low-beam operation of a buck controller using the A80803 device.

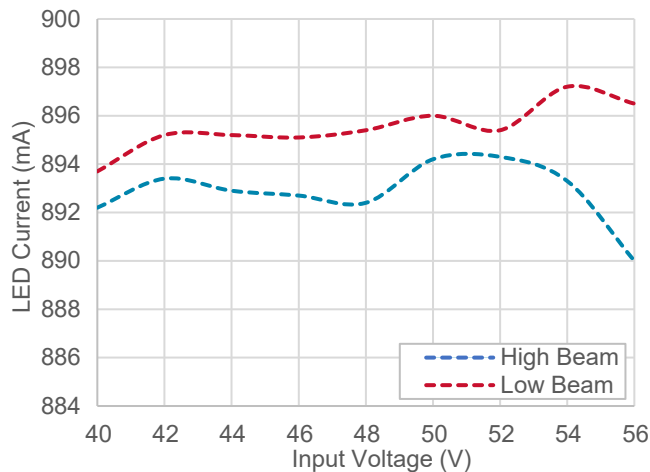


Figure 6: LED current vs. input voltage for high-beam and low-beam operation of a buck controller using the A80803 device.

The steady-state operation of the buck controller using the A80803 device in high-beam operation at the input voltage of 48 V is shown in Figure 7. As shown, the LED voltage—which is the difference between the anode voltage and the cathode voltage—is measured to be approximately 17.43 V for six LEDs. The A80803 device operates at a switching frequency ~ 350 kHz. Similarly, the operation of the buck controller in high-beam operation at the input voltage of 40 V and 56 V is shown in Figure 8 and Figure 9, respectively.

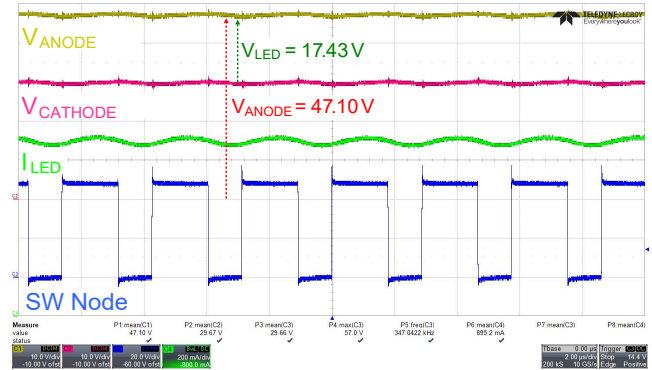


Figure 7: Steady-state operating waveform for six LEDs (high-beam operation) at an input voltage of 48 V.

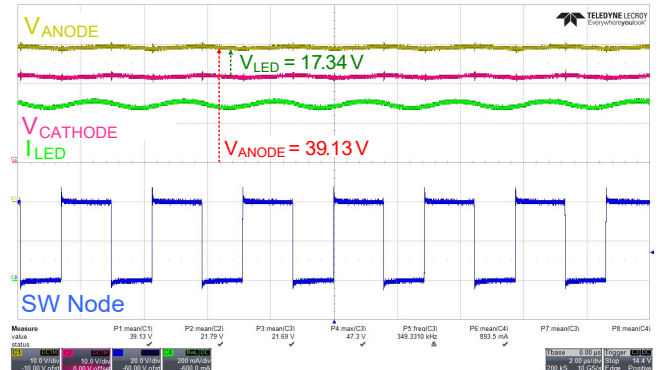


Figure 8: Steady-state operating waveform for six LEDs (high-beam operation) at an input voltage of 40 V.

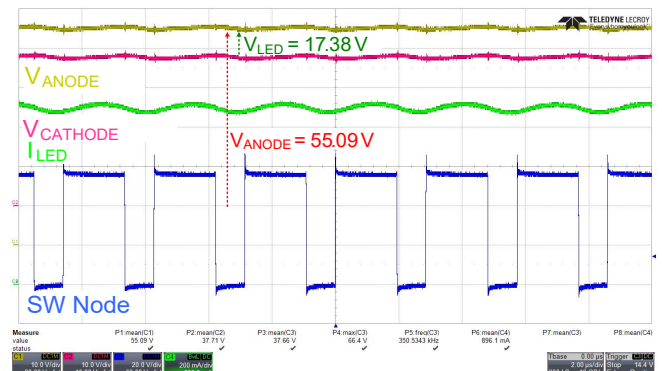


Figure 9: Steady-state operating waveform for six LEDs (low-beam operation) at an input voltage of 56 V.

The steady-state operation of the buck controller using the A80803 device in low-beam operation is shown in Figure 10, Figure 11, and Figure 12, at the input voltage of 48 V, 40 V and 56 V, respectively. As shown in these figures, the LED voltage drop of ~12 V (typical) is observed in low-beam operation for four LEDs in series, and the cathode voltage is adjusted by the buck controller to meet the LED voltage demand.

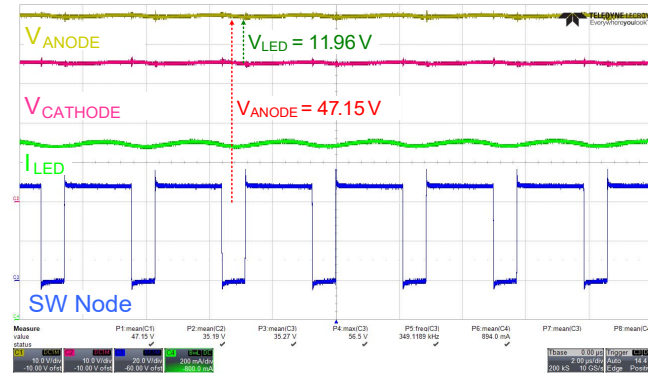


Figure 10: Steady-state operating waveform for four LEDs (low-beam operation) at an input voltage of 48 V.

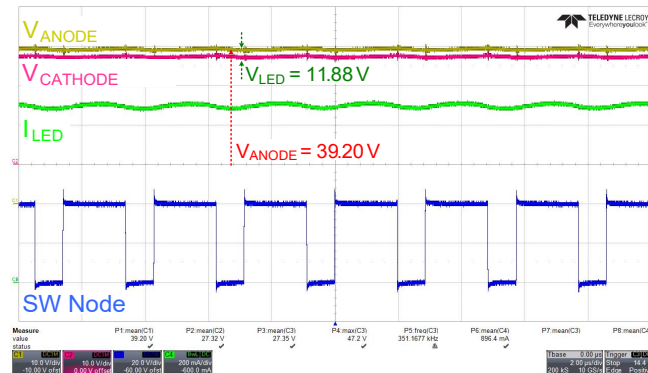


Figure 11: Steady-state operating waveform for four LEDs (low-beam operation) at an input voltage of 40 V.

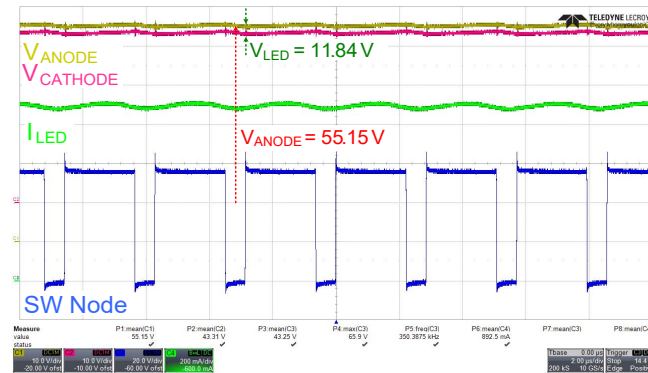


Figure 12: Steady-state operating waveform for four LEDs (low-beam operation) at an input voltage of 56 V.

Dimming

This section presents the steady-state operation of the buck controller during LED dimming using the internal PWM generator of the A80803 device.

The variation of the output power versus the duty ratio of the PWMOUT pin for high-beam and low-beam operation is shown in Figure 13. As shown, output power varies linearly with duty. The variation of the efficiency of the overall system with the variation of the duty of the PWMOUT pin is shown in Figure 14. Efficiency increases at the higher duty ratio.

Operation of the A80803 buck controller is shown in Figure 15 and Figure 16 at a PWM duty of 70% and 30%, respectively, with at a dimming frequency if 250 Hz.

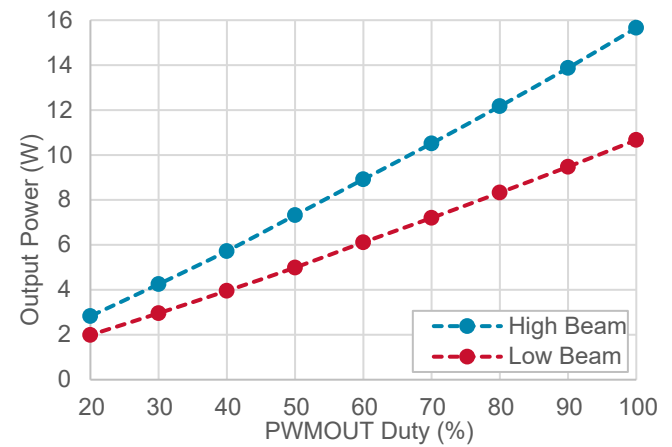


Figure 13: Output power vs. PWM duty for high-beam and low-beam operation of a buck controller using the A80803 device.

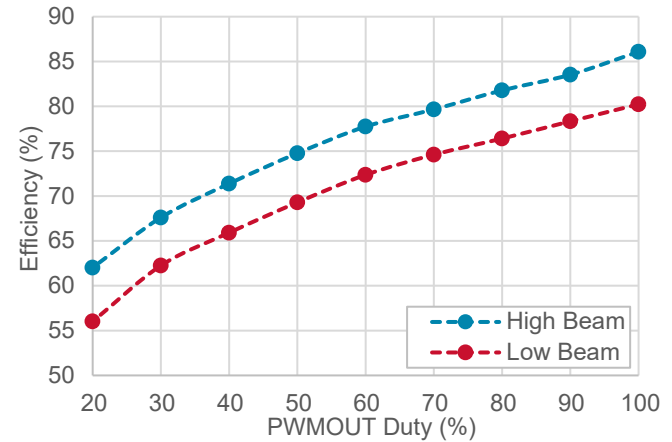


Figure 14: Efficiency vs. PWM duty for high-beam and low-beam operation of a buck controller using the A80803 device.

Thermals

Thermal images of the buck-controller board at a rated input voltage of 48 V driving six LEDs is shown in Figure 17 and driving four LEDs is shown in Figure 18. As shown,

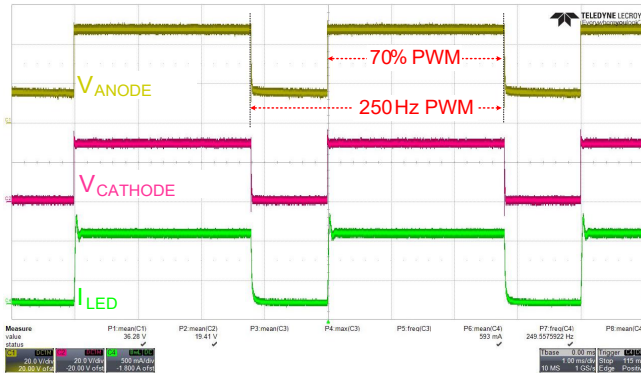


Figure 15: Dimming operation at 70% PWM duty for six LEDs (high-beam operation) at an input voltage of 48 V.

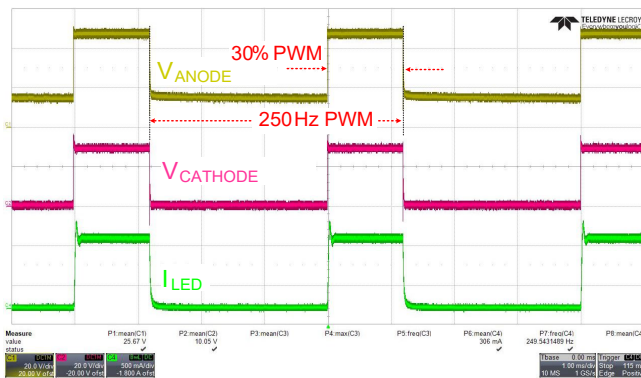


Figure 16: Dimming operation at 30% PWM duty for six LEDs (high-beam operation) at an input voltage of 48 V.

the maximum temperature on the board is approximately 67.9°C/63.8°C at room temperature with high-beam/low-beam operation.

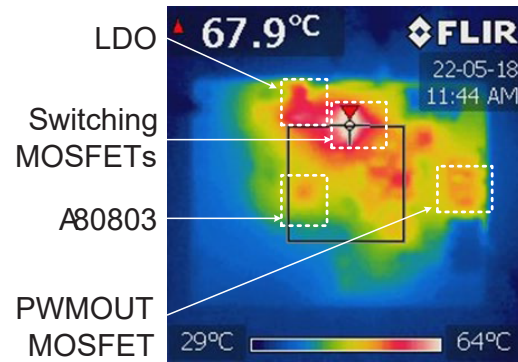


Figure 17: Thermal performance of high-beam operation (six LEDs) with a 48 V input at room temperature.

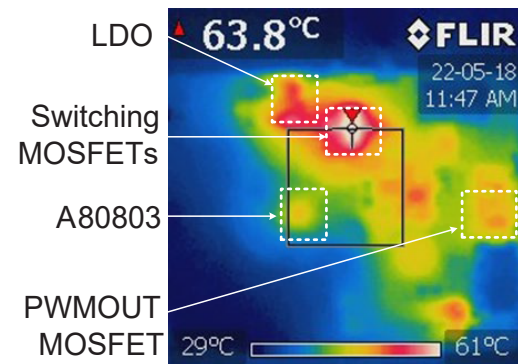


Figure 18: Thermal performance for high-beam operation (four LEDs) with a 48 V input at room temperature.

TRANSIENT OPERATION

Slew Control

This section presents operation of the A80803 buck controller with slew-rate control during the high-beam to low-beam transition and the low-beam to high-beam transition.

As previously discussed, the components R_{SLEW} and C_{SLEW} on the SLEW pin determine the rate of slew control of the LBG MOSFET, which controls the high-beam/low-beam operation. Operation of the A80803 buck controller with C_{SLEW} of 47 nF and 100 nF (R_{SLEW} fixed at 5 k Ω) during the transition from high-beam to low-beam operation is shown in Figure 19 and Figure 20, respectively. As shown, the cathode voltage increases gradually with a slew time of $\sim 900 \mu\text{s}$ and 1800 μs for a cathode voltage rise of $\sim 6.6 \text{ V}$. This corresponds to measured slew rates of 7.33 V/ms and 3.66 V/ms for the 47 nF and 100 nF capacitors (C_{SLEW}), per designed values, as shown in Equation 21 and Equation 22.

Similarly, operation of the A80803 buck controller with C_{SLEW} of 47 nF and 100 nF (R_{SLEW} fixed at 5 k Ω) during the transition from low-beam operation to high-beam operation is shown in Figure 21 and Figure 22, respectively. As shown, the slew rate achieved closely matches the designed values with good slew-rate control of the cathode voltage.

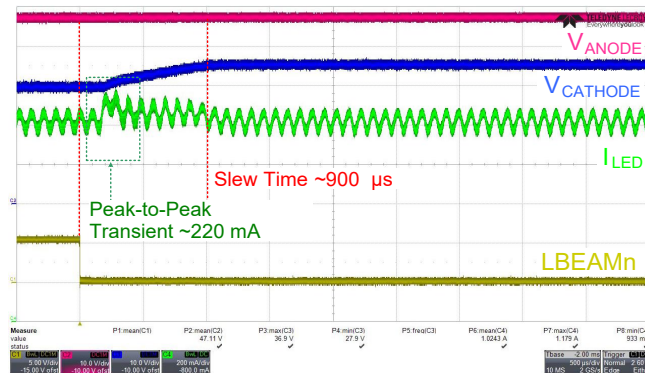


Figure 19: Transient behavior during the transition from high-beam operation to low-beam operation, with C_{SLEW} of 47 nF.

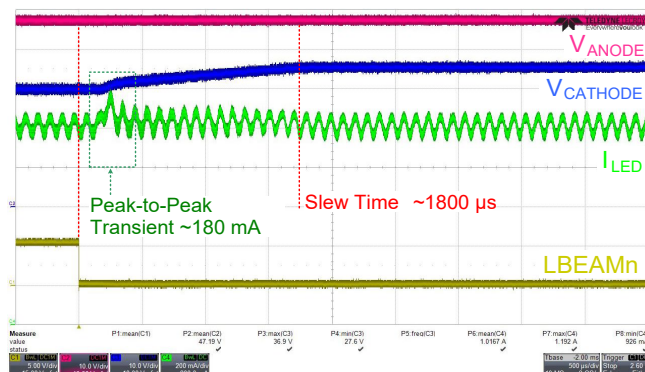


Figure 20: Transient behavior during the transition from high-beam operation to low-beam operation, with C_{SLEW} of 100 nF.

Operation of the slew-rate control in Figure 23 shows the variation of the cathode voltage (pink), voltage at the SLEW pin (blue), and gate voltage of the slew (SW_{LB}) MOSFET connected to the LBG node (green) with high-beam to low-beam transition signal (L_{BEAMn} , yellow). As shown, once the SLEW pin threshold of 250 mV is achieved, the controller starts to operate in the slew-control mode. In this mode, the gate of the slew control (SW_{LB}) operates in the Miller region, and the cathode voltage slews during this period. This timing is effectively controlled by the values of R_{SLEW} and C_{SLEW} .

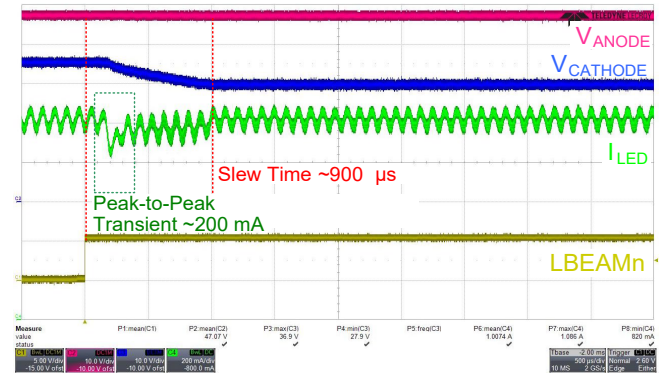


Figure 21: Transient behavior during low-beam to high-beam transition with C_{SLEW} as 47 nF.

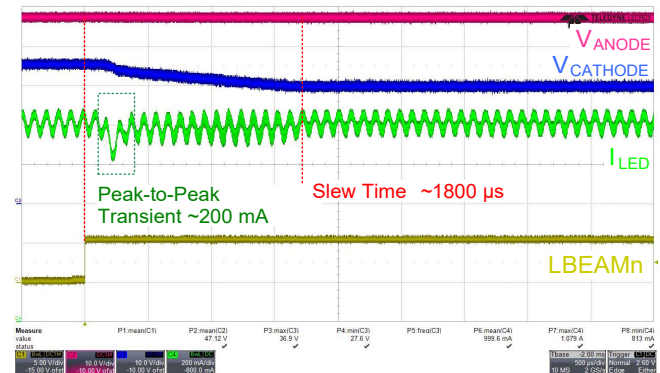


Figure 22: Transient behavior during the transition from low-beam operation to high-beam operation, with C_{SLEW} of 100 nF.

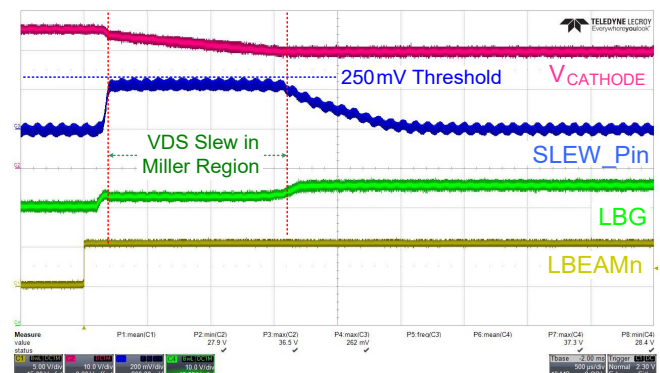


Figure 23: Transient behavior showing intermediate signals during the transition from high-beam operation to low-beam operation ($C_{SLEW} = 100 \text{ nF}$).

Simple Slew Control

This section presents operation of the A80803 buck controller with simple slew-rate control during the transitions from high-beam to low-beam operation and from low-beam to high-beam operation.

The circuit configuration of the A80803 buck controller with simple slew-rate control is shown in Figure 24. As shown, to disable slew-rate control, components on the SLEW pin are removed, and the SLEW pin is connected directly to ground. Moreover, for an additional cost benefit when there is no requirement for configuration of slew-rate control, the LDO regulator and the differential amplifier can also be eliminated in the circuitry.

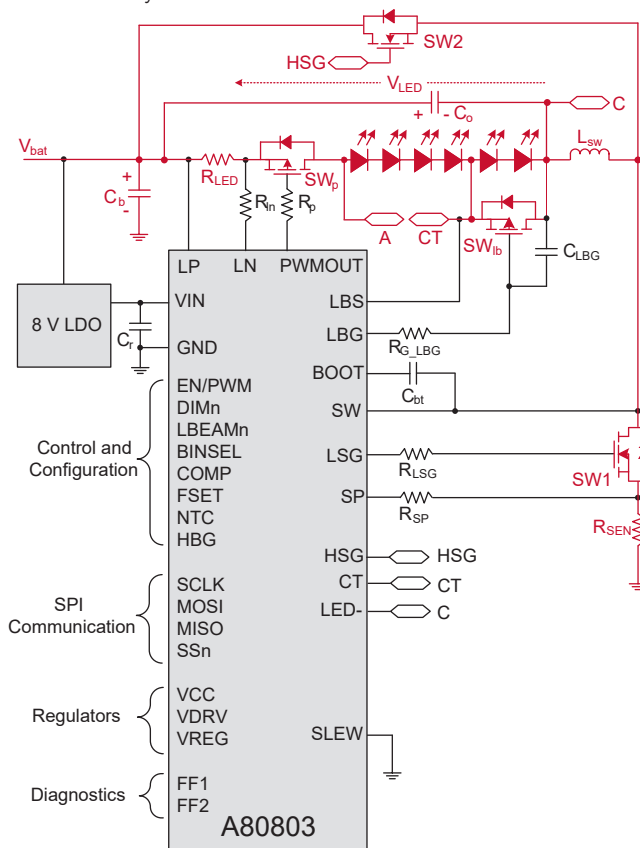


Figure 24: High-voltage buck configuration using A80803 with simple slew-rate control.

Transient operation of the A80803 buck controller with simple slew-rate control for the high-beam to low-beam transition and the low-beam to high-beam transition is shown in Figure 25 and Figure 26, respectively. The period of overshoot/undershoot of LED current increases from $<100 \mu\text{s}$ typically (Figure 19 through Figure 22) to $>400 \mu\text{s}$ (Figure 25 and Figure 26). Moreover, this undershoot/overshoot period is highly dependent on various external factors, such as the ambient temperature, which can lead to a longer duration of overshoot/undershoot. The extended duration of overshoot/undershoot of LED current can cause a flicker in the LED operation; this flicker is not present in the configuration with slew-rate control.

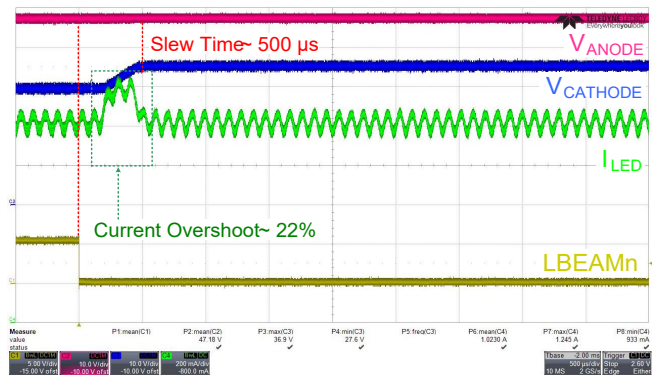


Figure 25: Transient behavior during the transition from high-beam operation to low-beam operation, with simple slew control.

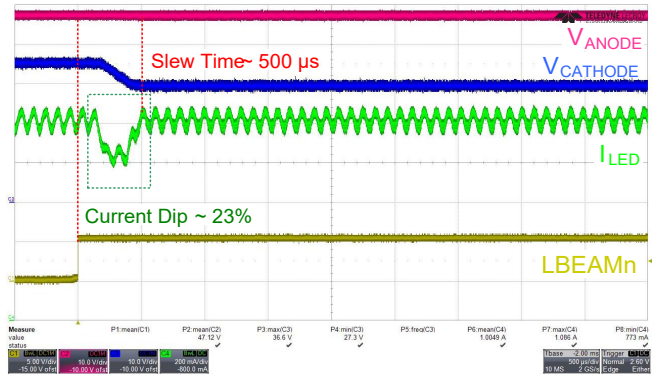


Figure 26: Transient behavior during transition from low-beam operation to high-beam operation, with simple slew control.

PROTECTION

The A80803 is a highly configurable device with numerous protection schemes. However, this section focusses on how the A80803 handles a single LED short, complete LED string short, and LED open fault during high-beam and low-beam operation.

Single-LED Short

A fault for a single-LED short is detected by two undervoltage comparators—one for each mode of operation (high-beam and low-beam). Comparator levels are programmable according to the number of LEDs. For this application, the undervoltage comparator settings are:

- High-Beam undervoltage (HB_OUT_UV) comparator between LP and LED- node (set at 16.8 V)
- Low-Beam undervoltage (LB_OUT_UV) comparator between LP and CT (set at 10.4 V)

Protection against the effects of a single-LED short during high-beam and low-beam operation is shown in Figure 27 and Figure 28, respectively. When a single LED is shorted:

- In high-beam operation, the typical LED voltage reduces from ~18 V to ~15 V. This trips the high-beam undervoltage (HB_OUT_UV) comparator, which has a threshold of 16.8 V.
- In low-beam operation, the typical LED voltage reduces from ~12 V to ~9 V. This trips the low-beam undervoltage (LB_OUT_UV) comparator, which has a threshold of 10.4 V.

As shown in these figures, reporting of high-beam and low-beam undervoltage faults is configured on the FF2 line, which shows a high-to-low transition after a minimum configured fault delay of 50 ms.

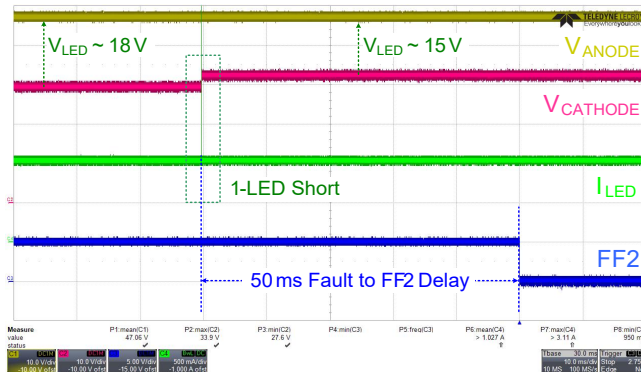


Figure 27: Device protection during a single-LED short during high-beam operation.

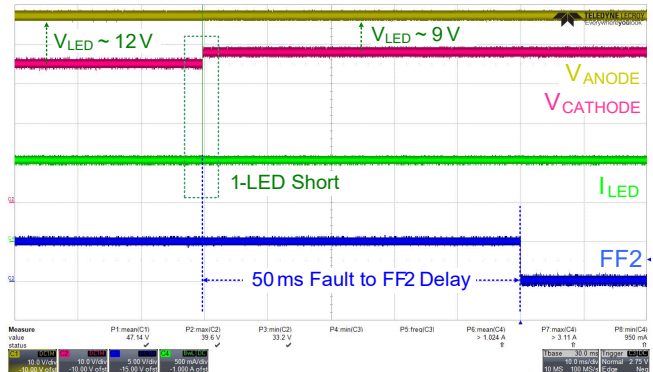


Figure 28: Device protection during a single-LED short during low-beam operation.

LED-String Short

A short of an LED string is detected if the voltage between the LP and CT terminals drops below 1 V while the PWM MOSFET is in the on state. As soon as this fault is detected, the low-side gate (LSG), high-side gate (HSG), and PWM MOSFET switch to the off state. The device restarts after a hiccup shutdown period (t_{HIC}) of 10 ms. If the fault is removed, the device operates in a nominal way; else, the device enters a low-side current limit operation and waits for 64 switching cycles to elapse before turning off the MOSFET for the hiccup shutdown period.

Protection against the effects of an LED-string short in high-beam and low-beam operation is shown in Figure 29 and Figure 30, respectively. As shown, as soon as the fault occurs, the device waits for the hiccup shutdown period to elapse before entering the low-side current-limit operation spanning 64 switching cycles. The fault pin transitions from high to low after a minimum configurable delay of 50 ms.

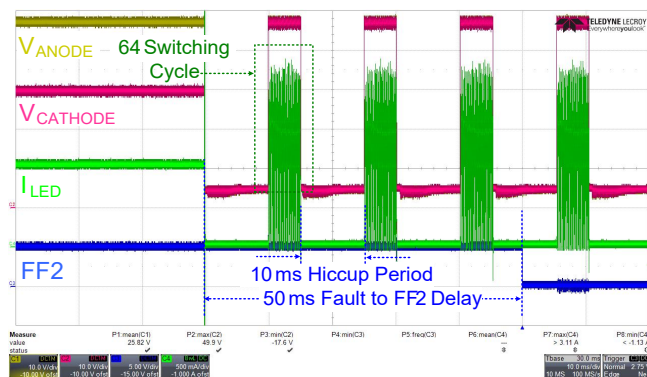


Figure 29: Device protection from the effects of a complete LED-string short during high-beam operation.

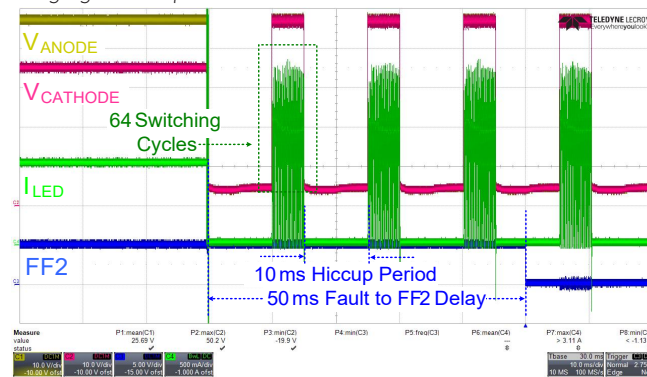


Figure 30: Device protection from the effects of a complete LED-string short during low-beam operation.

LED Open

An open LED fault is detected by two overvoltage comparators—one for each mode of operation (high-beam and low-beam). Comparator levels are programmable according to the number of LEDs. For this application, the overvoltage comparator settings are:

- High-Beam overvoltage (HB_OUT_OV) comparator between the LP and LED- nodes (set at 23.6 V)
- Low-Beam overvoltage (LB_OUT_OV) comparator between the LP and CT nodes (set at 15.2 V)

The LED-open scenario in high-beam operation is shown in Figure 31. As shown, cathode voltage drops suddenly, which trips the high-beam overvoltage comparator (HB_OUT_OV) present between the LP and LED- nodes. After a minimum configurable fault delay of 50 ms, LED current drops to zero and a fault is asserted. In this operation, the device shows an open LED, output overvoltage, and high-beam fault.

Similarly, the A80803 buck controller during low-beam operation is shown in Figure 32. The low-beam operation overvoltage comparator (LB_OUT_OV) trips due to voltage overshoot between the LP and CT nodes. The LED current reduces to zero and a fault is asserted on the fault pin after a delay of 50 ms.

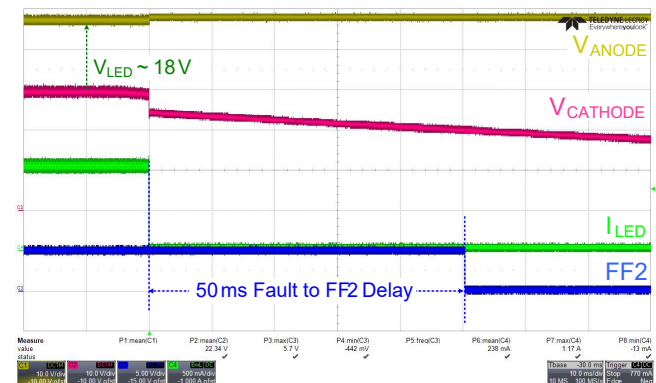


Figure 31: Device protection during LED open (between the anode and the CT node) during high-beam operation.

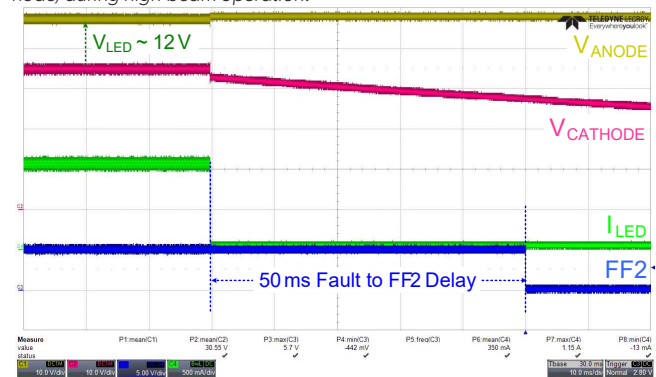


Figure 32: Device protection during LED open (between the anode and the CT node) during low-beam operation.

EXPERIMENTAL SETUP DETAILS

The developed PCB for the A80803 buck controller showing the pads where various components are placed as shown in Figure 33. This design can be used for automotive headlight applications where power is sourced directly from a 48 V power supply and can be extended to similar applications, such as taillights, stopping lights, and daylight running lights (DRL)/position lights. The circuit is configured in buck topology to operate at a 48 V input voltage range with input voltage variation from 40 V to 56 V.

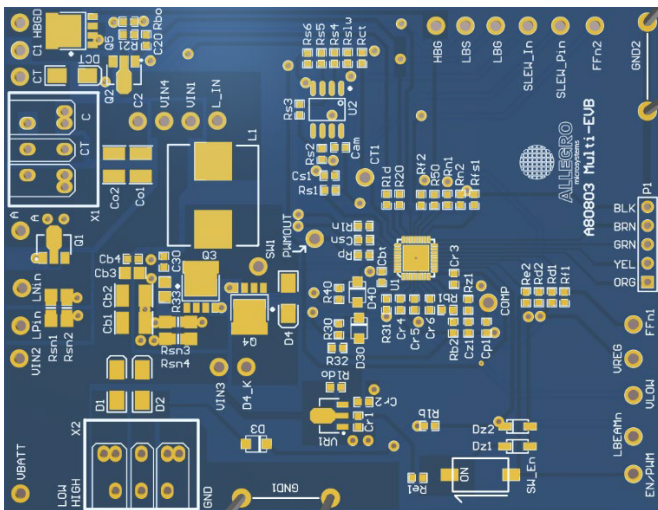


Figure 33: Developed PCB of the A80803 buck controller showing the component pads.

The developed experimental board to drive six serial LEDs in high-beam operation and four serial LEDs in low-beam operation using an A80803 buck controller is shown in Figure 33. Various components of the board—such as the switching inductor, switching MOSFETs, LBG and PWMOUT PMOS, differential amplifiers, LDO, programming connector, and various input/output terminals—are highlighted in Figure 34.

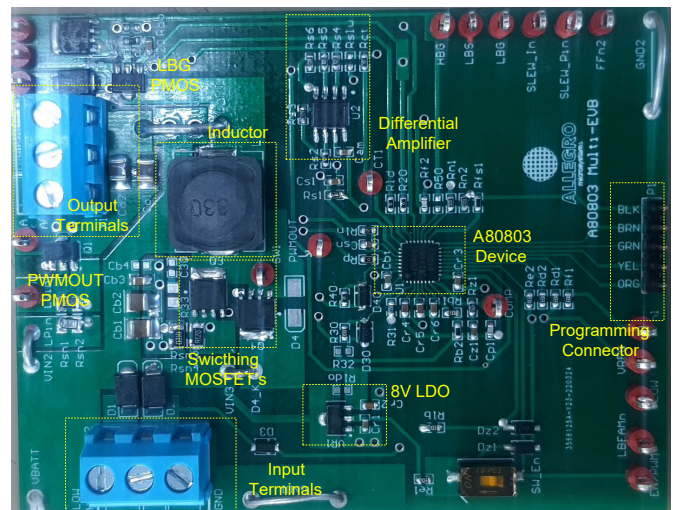


Figure 34: Developed experimental board of the A80803 buck controller showing various components.

SCHEMATIC AND BILL OF MATERIALS

The developed schematic for the high-voltage buck controller driving six LEDs in high-beam and four LEDs in low-beam with ~1000 mA LED current is shown in Figure 35. The schematic includes a complete circuit of the transition from high-beam operation to low-beam operation with power supply from a 48 V battery input voltage. For smooth transitions

between high-beam and low-beam operation, additional circuitry for the slew-rate control is provided.

A list of the complete bill of materials (BOM) for the developed board is provided in Table 1, which details two configurations of the buck controller—one with slew-rate control and the other with the simple slew option.

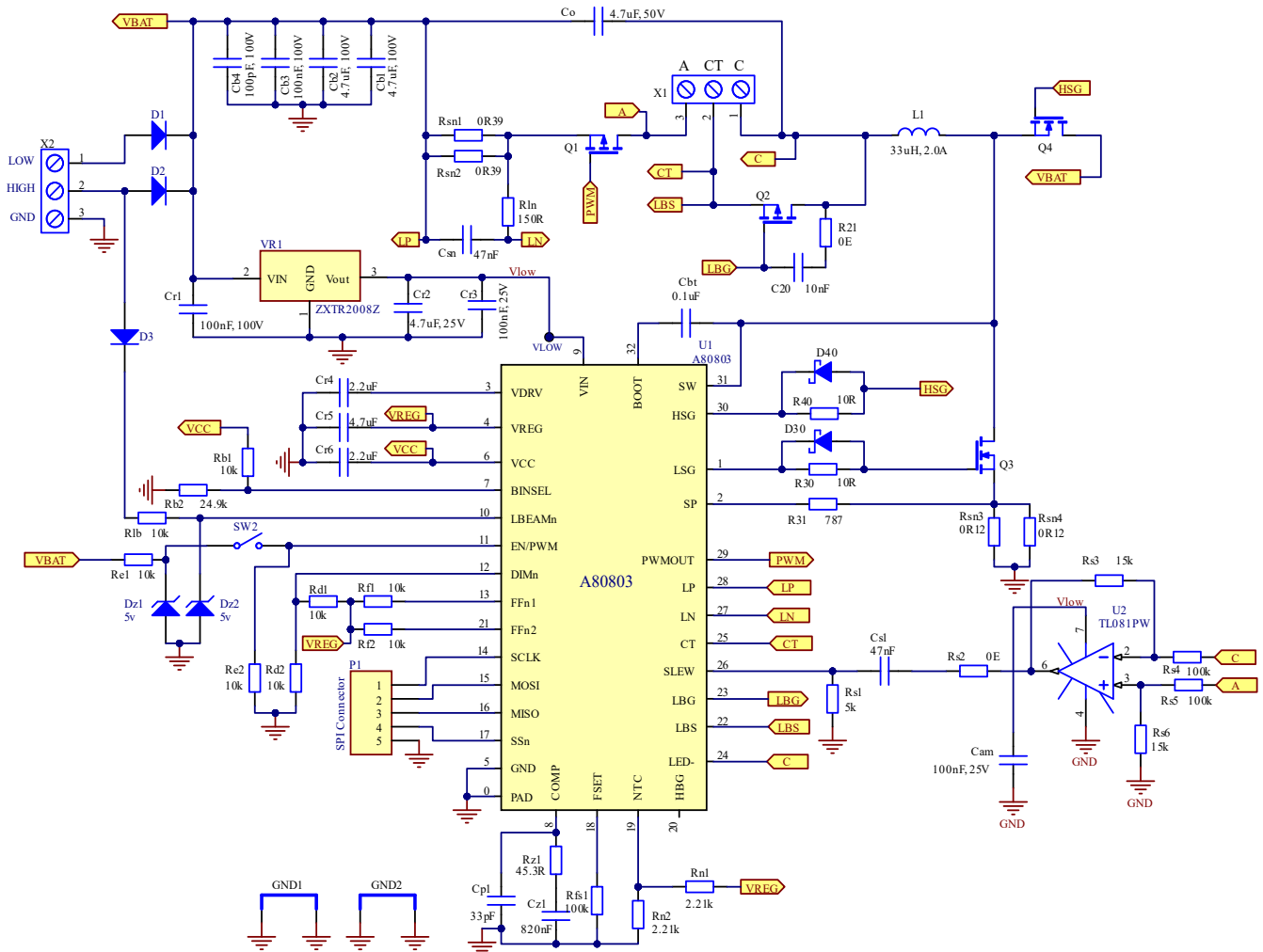


Figure 35: Schematic of the A80803 buck controller

Table 1: Bill of Materials for A80803 Buck Controller

	Designator	Footprint	Comment	Slew Control (Op-Amp)	Simple Slew Option
Input/Output Power Connection	Cb1, Cb2, Co1, Co2	1210	4.7 μ F, 100 V	4	4
	Cb3	0805	100 nF, 100 V	1	1
	Cb4	0603	100 pF, 100 V	1	1
	D1, D2	sma	100 V, 3 A	2	2
	X1, X2	BLOCK 3x	CON_200P	2	2
Regulator (Board and Device)	VR1	SOT89 LDO	ZXTR2008Z	1	1
	Cbt	0603	100 nF, 100 V	1	1
	Cr1	0603	100 nF, 100 V	1	1
	Cr2	0603	4.7 μ F, 25 V	1	1
	Cr3	0603	100 nF, 25 V	1	1
	Cr4, Cr6	0603	2.2 μ F, 25 V	2	2
Power-Switching	Rsn1, Rsn2	1206/0805	390 m Ω	2	2
	Csn	0603	47 nF, 25 V	1	1
	Rln	0603	150 Ω	1	1
	Q1, Q2	SOT89_P MOS	PCP1302, P-Ch	2	2
	R21	0603	2.4 k Ω	1	1
	C20	0603	4.7 nF, 25 V	1	1
	L1	SM_13.8x12.5	33 μ H, 2.0 A	1	1
	Q3, Q4	LFPAK56_2	BUK9Y65-N-ch	2	2
	R30, R40	0603	10 Ω	1	1
	D30, D40	SOD123W	100 V, 1 A	2	2
	R31	0603	787 Ω	1	1
Rsn3, Rsn4	1206/0805	120 m Ω	2	2	
Slew Components	Rs1	0603	5 k Ω /0 Ω	1 (5 k Ω)	1 (0 Ω)
	Cs1	0603	47 nF, 25 V	1	DNP
	Rs2	0603	0 Ω	1	DNP
	Cam	0603	100 nF, 25 V	1	DNP
	Rs3, Rs6	0603	15 k Ω	2	DNP
	Rs4, Rs5	0603	100 k Ω	2	DNP
	U2	PKG_SOIC8	TL081PW	1	DNP
A80803 Components	U1	MLPQ32_5x5	A80803	1	1
	Rb1, Rlb, Rd1, Rd2, Rf1, Rf2, Re1, Re2	0603	10 k Ω	8	8
	Rb2	0603	24.9 k Ω	1	1
	D3	SOD123W	100 V, 3 A	1	1
	Dz1, Dz2	SOD123/X.85	5 V Zener	2	2
	SW_En	SW DIP 1POS	SW-SPST	1	1
	Cp1	0603	33 pF, 25 V	1	1
	Cz1	0603	820 nF, 25 V	1	1
	Rz1	0603	45.3 Ω	1	1
	Rfs1	0603	100 k Ω	1	1
	Rn1, Rn2	0603	2.21 k Ω	2	2
P1	HDR1X5	Header 5	1	1	

CONCLUSION

This application note has presented an implementation of a high-input-voltage (48 V) buck controller for automotive applications such as headlights, tail-stop lights, and position lights/DRLs. The slew-rate control feature of the device has been explored in detail. The highly integrated A80803 device has numerous protection features, and this report has detailed:

- Implementation of a buck controller with slew-rate control.
- Device operation and design configuration of the slew-rate components.
- Differences in transient behaviors during high-beam to low-beam and low-beam to high-beam transitions, with and without slew-rate control.
- Device protection during various fault scenarios.
- Evaluation board schematics and bill of material (BOM).

ACKNOWLEDGEMENT

The authors would like to thank Nai-Chi Lee for continuous evaluation and provision of insight that greatly improved this application note.

REFERENCES

- [1] A80803, Multi-Topology LED Driver with PWM Dimming and Seamless High/Low Intensity Modes, Datasheet, Allegro MicroSystems, June 2021. <https://www.allegromicro.com/en/products/regulate/led-drivers/led-drivers-for-lighting/a80803>
- [2] A80803 Evaluation Board and Programming GUI, User Manual, Allegro MicroSystems, February 2022. https://www.allegromicro.com/-/media/files/application-notes/an296281-auto-led-headlamp-applications.pdf?sc_lang=en
- [3] LED Headlamps for Mainstream Vehicles: High/Low Beam LED Controller IC Solves Common Design Challenges, Allegro MicroSystems, October 2021. https://www.allegromicro.com/-/media/files/brochures/am035-led-headlamp-controller-ics.pdf?sc_lang=en&hash=9D73B0DCFBF2AAA0EFE13A1EF7F9EC7B
- [4] Nai-Chi Lee and Vijay Mangtani, Apparatus and Methods for LED Control, US Patent 9,781,789 B1, issued October 3, 2017. <https://patents.google.com/patent/US9781789B1/en>

Revision History

Number	Date	Description	Responsibility
-	September 19, 2023	Initial release	V. Bist, S. Wekhande

Copyright 2023, Allegro MicroSystems.

The information contained in this document does not constitute any representation, warranty, assurance, guaranty, or inducement by Allegro to the customer with respect to the subject matter of this document. The information being provided does not guarantee that a process based on this information will be reliable, or that Allegro has explored all of the possible failure modes. It is the customer's responsibility to do sufficient qualification testing of the final product to ensure that it is reliable and meets all design requirements.

Copies of this document are considered uncontrolled documents.